Journal of Sound and Vibration (2001) **242**(5), 867–891
doi:10.1006/jsvi.2000.3396, available online at http://www.idealibrary.com on IDEAL®

SYSTEM IDENTIFICATION AND MODEL REDUCTION FOR A SINGLE-LINK FLEXIBLE MANIPULATOR

K. Liu and X. Sun

Faculty of Engineering, Lakehead University, Thunder Bay, Ontario, Canada P7B 5E1,

(*Received* 13 *September* 1999, *and in final form* 19 *September* 2000)

A new model reduction and updating technique is proposed and applied in modelling of a single-link flexible manipulator. The Observability Range Space Extraction algorithm is used to generate an initial overparameterized state-space model. The identified model is transformed into modal realization. The modal responses of individual modes are evaluated. A new measure is proposed to quantify the contribution of individual modes to the total responses. Using the proposed measure, a reduced order model is obtained by retaining the most significant modes. To improve model accuracy, either the reduced input or output matrix can be recalculated by a proposed method. Several critical issues related to the experimental identification are addressed. Experimental identification results are presented to illustrate the proposed technique.

1. INTRODUCTION

Identification is the process of developing or improving a mathematical representation of a physical system using experimental data. Identification work can be classified as three types: modal parameter identification, structural-model parameter identification, and control-model identification [1]. In modal parameter identification, the dynamics of structures is characterized by modal parameters such as natural frequencies, damping ratios, and mode shapes. Using the identified modal parameters, additional processes can be performed to obtain structural-model parameters such as mass, damping, and stiffness matrices. Control-model identification finds a parametric model to represent a system in order to design a controller. In the context of this paper, identification refers to the control-model identification.

During the past two decades, numerous techniques for control-model identification have been developed in the control literatures. The methods to identify discrete-time state-space model have been receiving more and more attention as such a model is a popular choice for computer control of linear time-invariant systems. If a pulse response is available, the Eigensystem Realization Algorithm (ERA) can be directly applied to obtain the system parameter matrices [2, 3]. The recursive form of the ERA is developed for the purpose of on-line system identification [4]. For general response data, the Observer/Kalman filter identification algorithm (OKID) can be used and it consists of three steps, i.e., computation of the observer Markov parameters, recovery of the system and observer gain Markov parameters, and realization of a state-space model [1, 5]. The Observability Range Space Extraction (ORSE) algorithm [6] is developed by generalizing the Q-Markov Covariance Equivalent Realization (Q-Markov Cover) [7] and the ERA. The ORSE algorithm can obtain a state-space model directly from general input/output data. Unification of several system realization algorithms is discussed in reference [8]. In essence, the ERA, OKID, and

0022-460X/01/200867 + 25 $35.00/0

ORSE methods have their roots in subspace model identification (SMI) [9]. These methods have been successfully applied in the identification of large flexible space structures [10, 11].

A common feature of the algorithms such as the OKID or ORSE is that the model must be properly overparameterized in order to capture the dynamics of systems. This need arises due to the effects of irregularities such as measurement noise and non-linearities of actual systems. An overparameterized model contains both the system modes and computational modes. The order of the estimated model must be reduced to eliminate the computational modes and insignificant system modes. The reduced order model must be updated to correct errors caused by truncation of some modes. A procedure for model reduction and updating is proposed in reference [6]. The procedure employs the balanced realization (BR) technique to transfer the model into a balanced form such that the importance of each mode is indicated by its corresponding diagonal element of the joint Gramian matrix or Hankel singular value [12]. Then the less important modes are eliminated to produce a lower order model. Some problems have encountered when the BR technique is used to deal with identified models of the systems that contain both rigid and flexible modes. First, the BR technique requires that the models be asymptotically stable. For systems that contain both rigid and flexible modes, identified models may not be stable. Second, the BR technique judges the model quality in terms of the minimum error between the impulse responses of the models. Such a criterion tends to overemphasize lightly damped modes in the higher-frequency region. Third, determination of a threshold value for small Hankel singular values is more or less a matter of subjective judgement.

For model updating, an iterative least-squares (LS) model updating algorithm is used in reference [6]. The model to be updated is assumed to be sufficiently accurate so that the prediction error of the model can be approximated by the product of the gradient matrix and the parameter updating vector. The algorithm updates the elements of the parameter matrices iteratively until the prediction error cannot be further reduced. The iterative LS updating algorithm has a slow convergence because only the first order information is used. In reference [13], optimized system identification was achieved using sequential quadratic programming iterations. It starts the iterations with the model identified using the OKID algorithm. The process can be considered as a model updating operation. The optimization minimizes a non-linear function of many variables, i.e., the elements of the parameter matrices. Hence, it can converge to local minima.

The first objective of this study is to apply the ORSE algorithm to an electro-mechanical system that contains both rigid and flexible modes. Specifically, a single-link flexible manipulator is used as a test-bed for such system. Identification of flexible manipulators has been studied by many researchers. In reference [14], an autoregressive moving average (ARMA) model was used to model a single-link flexible manipulator. The recursive least-squares (RLS) algorithm was chosen as the identification method. On-line frequency domain information was used for control of a flexible-link robot with varying payload in reference [15]. The study reported in reference [16] identified an ARMA model for a two-link flexible manipulator. Time domain and frequency domain methods were employed for the identification of a single-link flexible manipulator [17]. A model analysis was conducted for a two-link flexible manipulator in reference [18]. A state-space model of a flexible arm was first derived by the RLS estimation of an ARMA model and then a model reduction was conducted using the BR technique in reference [19]. In reference [20] the transfer functions of a single-link flexible manipulator were first obtained using band-pass filtering and then the parameters of the transfer functions were estimated by non-linear curve fitting. It has been noted that there are few reports about direct identification of a state-space model for a flexible manipulator. In this regard, this study addresses several

critical issues that arise in the implementation of the ORSE algorithm in modelling of a flexible manipulator system.

The second objective of the study is to develop a new model reduction technique. As the system under study involves rigid-body motion and lightly damped structural modes, identified models are likely to be unstable. To overcome the aforementioned shortcomings of the BR technique, the study proposes to conduct the model reduction in modal co-ordinates. To quantify the mode dominance in the responses, a new index, referred to as the modal response magnitude (MRM), is proposed. The importance of individual modes is determined by the MRM index and the model is reduced accordingly.

The third objective of the study is to develop a new model updating scheme that is more efficient than the iterative LS model updating algorithm used in reference [6]. The low efficiency of this algorithm is due to simultaneously modifying all the elements of the system matrices using the gradient information. For such a large dimension optimization problem, the solution is likely to converge to a local minimum. Instead of updating all the parameter matrices simultaneously, the proposed method recalculates either the input or output matrix while keeping the other two unchanged. The calculation is done by solving a non-iterative LS problem.

The remainder of this paper is organized as follows. Section 2 presents a short discussion on mathematical modelling for the system under study. Section 3 briefly introduces the ORSE algorithm. Section 4 describes the experimental setup. Section 5 details the development of the new model reduction and updating procedure. Section 6 presents the results of the identification experiments. Section 7 gives a brief conclusion.

2. MATHEMATICAL MODEL

An experimental set-up for a single-link flexible manipulator is shown in Figure 1. The detail of the set-up is described in section 4. Many studies on mathematical modelling of flexible manipulators have been reported. Although the present study intends to obtain a system model through identification, a brief discussion on mathematical modelling is beneficial for design of the experiment and interpretation of the results. To simplify the discussion, the flexible arm is modelled as a cantilever beam clamped to the rotational axis of the hub driven by a torque. The following assumptions are used.

(1) The link is uniform along its longitudinal direction, both in its mass distribution and elastic properties.
(2) The transverse shear stresses and the change in the moment of inertia due to elastic deformation are negligible, i.e., Euler's beam theory is applicable.
(3) The elastic deformation of the link is very small with respect to the hub motion.
(4) The link moves in a horizontal plane and hence, there is no effect of gravity.

Application of Lagrange's equations with respect to the hub motion results in

$$(I_h + I_\theta)\ddot{\theta} + \mathbf{I}_{\theta q}^{\mathrm{T}}\ddot{q} + 2q^{\mathrm{T}}\mathbf{I}_q\dot{q}\dot{\theta} + q^{\mathrm{T}}\mathbf{I}_q q\ddot{\theta} = \tau, \tag{1}$$

where θ is a scalar representing the angular position of the hub, q is a column vector representing the generalized co-ordinates of the flexural deformation of the link, τ is the torque applied at the hub, I_h is the effective moment of inertia of the hub including the counterweight, I_θ is the moment of inertia of the rigid arm and payload, I_q is a square matrix representing inertial effects of the distributed mass of the link and the payload mass due to the flexibility of the link, $\mathbf{I}_{\theta q}$ is a column vector representing the inertial effects caused by

coupling of the hub motion and the arm vibration. Application of Lagrange's equations with respect to the generalized co-ordinates results in

$$\mathbf{I}_{\theta q}\ddot{\theta} + \mathbf{I}_{\phi}\ddot{q} - \mathbf{I}_{\phi}\dot{\theta}^2 q + \mathbf{K}_q q = 0, \tag{2}$$

where $\mathbf{K}_q$ is a square matrix representing the effects of the distributed elasticity of the flexible link. Equations (1) and (2) are a set of non-linear differential equations. By neglecting higher order terms and assuming that damping is proportional to the velocity of the co-ordinates, the equations can be formulated as a matrix equation,

$$\mathbf{M}_{\phi}\ddot{\phi} + \mathbf{D}_{\phi}\dot{\phi} + \mathbf{K}_{\phi}\phi = f, \tag{3}$$

where

$$\mathbf{M}_{\phi} = \begin{bmatrix} I_h + I_{\theta} & \mathbf{I}_{\theta q}^{\mathrm{T}} \\ \mathbf{I}_{\theta q} & \mathbf{I}_q \end{bmatrix}, \quad \mathbf{D}_{\phi} = \mathrm{diag}\,[D_{\theta} \quad D_1 \quad D_2 \cdots], \quad \mathbf{K}_{\phi} = \begin{bmatrix} 0 & \mathbf{0} \\ \mathbf{0} & \mathbf{K}_q \end{bmatrix},$$

$$\phi = [\theta \quad q^{\mathrm{T}}], \quad f = [\tau \quad 0 \quad 0 \cdots]^{\mathrm{T}},$$

where D_{θ} is the damping coefficient corresponding to the hub's angle θ and D_i is the damping coefficient corresponding to the ith generalized co-ordinate q_i. It should be noted that the dynamics of the motor and transmission train is not included in the above equations.

Equation (3) can be transferred into a state-space equation by introducing a set of state variables

$$\dot{x}(t) = \mathbf{A}_c x(t) + \mathbf{B}_c u(t), \quad y(t) = \mathbf{C}_c x(t) + \mathbf{D}_c u(t), \tag{4}$$

where $x(t) \in R^{n\times 1}$ is the system state variable, $\mathbf{A}_c \in R^{n\times n}$ is the state transition matrix, $\mathbf{B}_c \in R^{n\times 1}$ is the input influence matrix, $\mathbf{C}_c \in R^{n\times 1}$ is the output influence matrix, $\mathbf{D}_c \in R^{m\times 1}$ is the direct transmission matrix, $\mathbf{y}(t) \in R^{m\times 1}$ is the output vector, n is the number of the state variables or the model order, and m is the number of outputs. The notation $R^{i\times j}$ represents the $i \times j$ real matrix space. For a digital control system, outputs are sampled at discrete times and input $u(t)$ is generated from a series of discrete signals. If the interval between two consecutive sampling points is Δt, equation (4) can be represented by a discrete-time state-space model,

$$x(k+1) = \mathbf{A}x(k) + \mathbf{B}u(k), \quad y(k) = \mathbf{C}x(k) + \mathbf{D}u(k), \tag{5}$$

where

$$\mathbf{A} \triangleq \mathrm{e}^{\mathbf{A}_c \Delta t}, \quad \mathbf{B} \triangleq \int_0^{\Delta t} \mathrm{e}^{\mathbf{A}_c \tau}\mathbf{B}_c\, d\tau, \quad \mathbf{C} \triangleq \mathbf{C}_c, \quad \mathbf{D} \triangleq \mathbf{D}_c,$$

$$x(k) \triangleq x(k\Delta t), \quad u(k) \triangleq u(k\Delta t), \quad y(k) \triangleq y(k\Delta t).$$

The state variables can be transformed into a new set of state variables through a co-ordinate transformation

$$x(k) = \mathbf{T}z(k), \tag{6}$$

where $\mathbf{T} \in R^{n\times n}$ is any non-singular matrix. Substitution of equation (6) into equation (5) yields

$$z(k+1) = \bar{\mathbf{A}}z(k) + \bar{\mathbf{B}}u(k), \quad y(k) = \bar{\mathbf{C}}z(k) + \mathbf{D}u(k), \tag{7}$$

where

$$\bar{\mathbf{A}} = \mathbf{T}^{-1}\mathbf{A}\mathbf{T}, \quad \bar{\mathbf{B}} = \mathbf{T}^{-1}\mathbf{B}, \quad \bar{\mathbf{C}} = \mathbf{C}\mathbf{T}. \tag{8}$$

3. IDENTIFICATION ALGORITHM

This section presents a brief introduction to the ORSE algorithm [6]. In experiment, the output $y(k)$ is contaminated by unknown measurement noise $w(k)$ giving the measured output $\tilde{y}(k)$,

$$\tilde{y}(k) = y(k) + w(k). \tag{9}$$

This system identification determines the matrices $\bar{\mathbf{A}}$, $\bar{\mathbf{B}}$, $\bar{\mathbf{C}}$, and $\mathbf{D}$ using the following data samples from experiments:

$$\tilde{y}(k) \quad \text{and} \quad u(k) \quad \text{for } k = 1, 2, \ldots, K,$$

where for a general multi-input/multi-output system, $u(k) \in R^{r\times 1}$ and $\mathbf{B}$ or $\bar{\mathbf{B}} \in R^{n\times r}$, $\mathbf{D} \in R^{m\times r}$. The ORSE algorithm starts with forming two Hankel matrices $\mathbf{Y} \in R^{qm\times d}$ and $\mathbf{U} \in R^{qr\times d}$ using data $\tilde{y}(k)$ and $u(k)$:

$$\mathbf{Y} = [\tilde{y}_q(1), \quad \tilde{y}_q(2), \ldots, \tilde{y}_q(d)]$$

$$= \begin{bmatrix} \tilde{y}(1) & \tilde{y}(2) & \cdots & \tilde{y}(d) \\ \tilde{y}(2) & \tilde{y}(3) & \cdots & \tilde{y}(d+1) \\ \vdots & \vdots & \ddots & \vdots \\ \tilde{y}(q) & \tilde{y}(q+1) & \cdots & \tilde{y}(K) \end{bmatrix}, \tag{10}$$

$$\mathbf{U} = [u_q(1), \quad u_q(2), \ldots, u_q(d)]$$

$$= \begin{bmatrix} u(1) & u(2) & \cdots & u(d) \\ u(2) & u(3) & \cdots & u(d+1) \\ \vdots & \vdots & \ddots & \vdots \\ u(q) & u(q+1) & \cdots & u(K) \end{bmatrix}, \tag{11}$$

where q and $d = K - q + 1$ is the block row dimension and the column dimension of the Hankel matrices respectively. If the output is free of measurement noise, the two Hankel matrices are related by the matrix equation

$$\mathbf{Y} = \mathbf{O}_q\mathbf{X} + \mathbf{H}_q\mathbf{U}, \tag{12}$$

where $\mathbf{O}_q \in R^{qn\times n}$ is referred to as the observability matrix which is of the form

$$\mathbf{O}_q = \begin{bmatrix} \mathbf{C} \\ \mathbf{C}\mathbf{A} \\ \vdots \\ \mathbf{C}\mathbf{A}^{q-1} \end{bmatrix}, \tag{13}$$

the matrix $\mathbf{X} \in R^{n \times d}$ is formed by the unknown state vectors

$$\mathbf{X} = [x(1), \quad x(2), \ldots, x(d)], \tag{14}$$

and the matrix $\mathbf{H}_q \in R^{qm \times qr}$ is defined as

$$\mathbf{H}_q = \begin{bmatrix} \mathbf{D} & 0 & \cdots & 0 \\ \mathbf{CB} & \mathbf{D} & \cdots & 0 \\ \mathbf{CAB} & \mathbf{CB} & \cdots & 0 \\ \vdots & \vdots & \ddots & 0 \\ \mathbf{CA}^{q-2}\mathbf{B} & \mathbf{CA}^{q-3}\mathbf{B} & \cdots & \mathbf{D} \end{bmatrix}. \tag{15}$$

The observability range space of order q of the state-space model (5) is defined as the range space of matrix $\mathbf{O}_q$, i.e.,

$$\text{range}(\mathbf{O}_q) = \mathbf{O}_q\mathbf{T} = \begin{bmatrix} \mathbf{CT} \\ \mathbf{CAT} \\ \vdots \\ \mathbf{CA}^{q-1}\mathbf{T} \end{bmatrix} = \begin{bmatrix} \bar{\mathbf{C}} \\ \bar{\mathbf{C}}\bar{\mathbf{A}} \\ \vdots \\ \bar{\mathbf{C}}\bar{\mathbf{A}}^{q-1} \end{bmatrix}, \tag{16}$$

for some non-singular matrix $\mathbf{T}$. In order to extract the observability range space from the relation (12), the part of the output $\mathbf{Y}$ that does not emanate from the state $\mathbf{X}$ needs to be eliminated. In other words, the second term on the right-hand side of equation (12) must be forced to be zero. To achieve this, a matrix $\mathbf{U}^{\perp} \in R^{d \times d}$ is needed such that $\mathbf{U}^{\perp}$ is normal to $\mathbf{U}$ or $\mathbf{U}\mathbf{U}^{\perp} = 0$. A simple formulation of $\mathbf{U}^{\perp}$ is given by

$$\mathbf{U}^{\perp} = \mathbf{I} - \mathbf{U}^{\mathrm{T}}(\mathbf{U}\mathbf{U}^{\mathrm{T}})^{+}\mathbf{U}, \tag{17}$$

where $\mathbf{I} \in R^{d \times d}$ is an identity matrix and the superscript $+$ denotes the Moore–Penrose pseudo-inverse. Postmultiplying equation (12) by $\mathbf{U}^{\perp}$ results in

$$\mathbf{Y}\mathbf{U}^{\perp} = \mathbf{O}_q\mathbf{X}\mathbf{U}^{\perp}. \tag{18}$$

Now the observability range space can be extracted by a singular-value decomposition (SVD) of the matrix $\mathbf{Y}\mathbf{U}^{\perp}$. In practice, observability range space is extracted by the SVD of the matrix $\mathbf{Y}\mathbf{Y}^{\mathrm{T}} - \mathbf{Y}\mathbf{U}^{\mathrm{T}}(\mathbf{U}\mathbf{U}^{\mathrm{T}})^{+}(\mathbf{Y}\mathbf{U}^{\mathrm{T}})^{\mathrm{T}}$ to reduce the computational time. It is easy to see that $\mathbf{Y}\mathbf{U}^{\perp}\mathbf{Y}^{\mathrm{T}} = \mathbf{Y}\mathbf{Y}^{\mathrm{T}} - \mathbf{Y}\mathbf{U}^{\mathrm{T}}(\mathbf{U}\mathbf{U}^{\mathrm{T}})^{+}(\mathbf{Y}\mathbf{U}^{\mathrm{T}})^{\mathrm{T}}$. The transition matrix $\bar{\mathbf{A}}$ and output matrix $\bar{\mathbf{C}}$ can be found from the extracted observability range space. Finally, the matrices $\bar{\mathbf{B}}$ and $\mathbf{D}$ can be obtained by a LS solution. It should be noted that the ORSE method is very similar to the method named as system realization using information matrix (SRIM) in reference [21] and the relation between the SRIM algorithm and the SMI algorithm is given in reference [8]. A detailed development of the SMI algorithm can be found in reference [9].

4. EXPERIMENTAL SET-UP

An experimental set-up used in this study is shown in Figure 1. The system consists of a flexible arm, a bevel gear set, a direct current (DC) motor with the power amplifier unit,

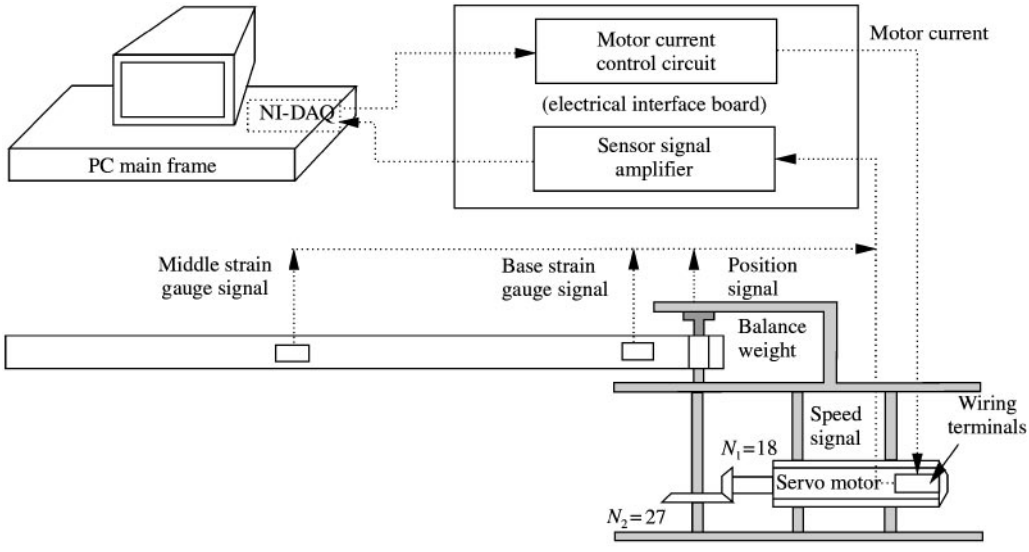

Figure 1. The experimental set-up.

and PC. The arm is constructed from 6061-T6 aluminum–magnesium–silicon alloy. Its dimension is length × height × width = $1 \times 0{\cdot}051 \times 0{\cdot}003$ m. The arm rotates in the horizontal plane to eliminate the influence of gravity. A counterweight is used to reduce unbalance of the arm.

The motor used in this experimental set-up is a permanent magnet DC motor with a rated stall torque of 2·938 Nm. The DC motor has an integral tachometer to measure motor shaft speed. To reduce noise in tachometer signal, an analog filter is used. A potentiometer is attached to the arm hub to measure its angular position. The control input available is a voltage signal that is proportional to the motor current. A power amplifier circuitry converts the input voltage from the computer to motor current. The maximum magnitude of the current is restricted to be 5 A.

Vibrations of the arm are measured using two sets of strain gauges or Wheatstone bridges. The first bridge is located near the clamped end of the arm. The voltage signal from this bridge is referred to as the base-gauge signal. The second bridge is placed in the middle of the arm. The signal from this bridge is referred to as the middle gauge signal. The strain gauge signals are amplified before being fed into the computer.

The computer used to control the system is a Pentium II with a speed of 200 MHz. A National Instruments PCI-MIO-16E-4 data-acquisition board is used for real-time control. The broad has 16 single-ended or eight differential analog inputs, two analog outputs, eight digital IOs, and two counters, and 12-bit resolution. The maximum sampling rate of the board is 500,000 samples/s. LabWindows by National Instruments is used for programming.

Totally, there are four system outputs, namely, the angular-position of the arm hub, the angular speed of the motor shaft, the base gause signal (the arm deflection near the clamped end), and the middle gauge signal (the arm deflection at the middle location). The experimental set-up is, therefore, a system with a single input and four outputs, i.e., $r = 1$ and $m = 4$. It is also noted that the direct transmission matrix $\mathbf{D}$ is zero because the outputs are not directly related to the input.

5. MODEL REDUCTION AND UPDATING

In this section, a new procedure is developed to reduce the identified model and improve the accuracy of the reduced order model. The main feature of the proposed procedure is that the model reduction and updating are conducted in modal co-ordinates. An eigendecomposition is conducted on the identified transition matrix

$$\bar{\mathbf{A}} = \mathbf{\Psi} \Lambda \mathbf{\Psi}^{-1}, \tag{19}$$

where

$$\mathbf{\Psi} = [\psi_1 \;\; \psi_2 \cdots \psi_{n_1-1} \;\; \psi_{n_1} \;\; \psi_{n_1+1} \cdots \psi_n] \in C^{m \times n}$$

is the eigenvector matrix and

$$\Lambda = \mathrm{diag}[\lambda_1 \;\; \lambda_2 \cdots \lambda_{n_1-1} \;\; \lambda_{n_1} \;\; \lambda_{n_1+1} \cdots \lambda_n] \in C^{m \times n}$$

is the eigenvalue matrix. The notation $C^{i \times j}$ represents the $i \times j$ complex matrix space. It is assumed that there are $n_1/2$ pairs of complex eigenvalues are eigenvectors, i.e., $\lambda_{i+1} = \lambda_i^*$, $\psi_{i+1} = \psi_i^*$ for $i = 1, 3, \ldots, n_1 - 1$, where the superscript $*$ denotes complex conjugate. The remaining $n - n_1$ eigenvalues and eigenvectors are real. Defining a set of new states in modal co-ordinates as

$$\eta(k) = \mathbf{\Psi}^{-1} z(k), \tag{20}$$

the state-space model becomes

$$\eta(k+1) = \Lambda \eta(k) + \hat{\mathbf{B}} u(k), \quad \hat{y}(k) = \hat{C} \eta(k), \tag{21}$$

where

$$\hat{\mathbf{B}} = \mathbf{\Psi}^{-1} \bar{\mathbf{B}} = [\hat{b}_1 \;\; \hat{b}_2 \cdots \hat{b}_{n_1-1} \;\; \hat{b}_{n_1} \;\; \hat{b}_{n_1+1} \cdots \hat{b}_n]^{\mathrm{T}} \in C^{n \times 1},$$

$$\hat{\mathbf{C}} = \bar{\mathbf{C}} \mathbf{\Psi}^{-1} = [\hat{c}_1 \;\; \hat{c}_2 \cdots \hat{c}_{n_1-1} \;\; \hat{c}_{n1} \;\; \hat{c}_{n_1+1} \cdots \hat{c}_n]^{\mathrm{T}} \in C^{m \times n}.$$

It is noted that complex quantities appear as pairs, i.e., $\hat{b}_{i+1} = \hat{b}_i^*$ and $\hat{c}_{i+1} = \hat{c}_i^*$ for $i = 1, 3, \ldots, n_1 - 1$.

An important question is how to distinguish the system modes from the computational modes. It is reasonable to assert that the computational modes have insignificant contribution to the total system response. To characterize the contribution of individual modes to the outputs, a quantitative measure is needed. Two indices are introduced in reference [1] to quantify the contribution of individual modes to a pulse response. The modal amplitude coherence (MAC) measures the correlation between the pulse responses extracted from the data and the pulse response generated by the identified model. The mode singular value (MSV) measures the magnitude of the pulse response generated by the identified model. Specifically, the MSV is defined as

$$\mathrm{MSV}_i = \sqrt{|\hat{c}_i|(1 + |\lambda_i| + |\lambda_i^2| + \cdots + |\lambda_i^{K-2}|)|\hat{b}_i|}. \tag{22}$$

A mode with a large MSV is considered to have a significant contribution to the pulse response. The computational modes and insignificant structural modes are expected to have small MSVs. The MAC or MSV may be misleading because it is based on the pulse response. For example, the pulse response of a mode with heavy damping or $|\lambda_i| \ll 1$ may die quickly even if the mode is one of the significant system modes when the system is

persistently excited. To overcome this problem, an alternative measure is proposed in this study. The system response is a sum of the modal responses, i.e.,

$$\hat{y}(k) = \sum_{i=1,3}^{n_1-1} \hat{y}_{\eta_i}(k) + \sum_{i=n_1+1}^{n} \hat{y}_{\eta_i}(k), \tag{23}$$

where $\hat{y}_{\eta_i}(k) \in R^{m\times 1}$ is the response of the ith mode. For the ith complex mode, $\hat{y}_{\eta_i}(k)$ is evaluated by

$$\begin{bmatrix} \eta_i(k+1) \\ \eta_i^*(k+1) \end{bmatrix} = \begin{bmatrix} \lambda_i & 0 \\ 0 & \lambda_i^* \end{bmatrix} \begin{bmatrix} \eta_i(k) \\ \eta_i^*(k) \end{bmatrix} + \begin{bmatrix} \hat{b}_i \\ \hat{b}_i^* \end{bmatrix} u(k),$$

$$\hat{y}_{\eta_i}(k) = [\hat{c}_i \quad \hat{c}_i^*] \begin{bmatrix} \eta_i(k) \\ \eta_i^*(k) \end{bmatrix}, \quad i = 1, 3, \ldots, n_1 - 1. \tag{24}$$

For the ith real mode, $\hat{y}_{\eta_i}(k)$ is evaluated by

$$\eta_i(k+1) = \lambda_i \eta_i(k) + \hat{b}_i u(k), \quad \hat{y}_{\eta_i}(k) = \hat{c}_i \eta_i(k), \quad i = n_1 + 1, \ldots, n. \tag{25}$$

The maximum contribution of the ith mode to the total response can be evaluated by a modal response magnitude (MRM) defined as

$$\mathrm{MRM}_i = \max\left(\sum_{k=1}^{K} |\hat{y}_{\eta_i}(k)|/K \right), \quad i = 1, 3, \ldots, n_1 + 1, n_1 + 1, \ldots, n. \tag{26}$$

The MRM computes the largest means of the absolute modal responses to the actual input. The modes with small MRMs can be considered to be insignificant. A reduced order model can be obtained by eliminating the matrix elements that correspond to the insignificant modes. The MRMs are more meaningful than the Hankel singular values used in the BR technique because each MRM is evaluated using its modal response to the actual input while a Hankel singular value measures the impulsive response magnitude of the corresponding mode. With the MRMs, a knowledge of the system dynamics from an analytical model or modal testing can be easily incorporated in decision making.

The reduced model has a triplet

$$\Lambda = \mathrm{diag}[\lambda_1 \;\; \lambda_2 \cdots \lambda_{n_1'-1} \;\; \lambda_{n_1'} \;\; \lambda_{n_1'+1} \cdots \lambda_{n'}] \in C^{n'\times n'}, \tag{27}$$

$$\hat{\mathbf{B}} = [\hat{b}_1 \;\; \hat{b}_2 \cdots \hat{b}_{n_1'-1} \;\; \hat{b}_{n_1'} \;\; \hat{b}_{n_1'+1} \cdots \hat{b}_{n'}] \in C^{n'\times 1}, \tag{28}$$

$$\hat{\mathbf{C}} = [\hat{c}_1 \;\; \hat{c}_2 \cdots \;\; \hat{c}_{n_1'-1} \;\; \hat{c}_{n_1'} \;\; \hat{c}_{n_1'+1} \cdots \hat{c}_{n'}] \in C^{m\times n'}, \tag{29}$$

where $n' < n$ denotes the order of the reduced model and n_1' denotes the number of complex modes. The reduced order model is expected to be less accurate than the original model. This problem can be corrected by recalculating the reduced matrices $\hat{\mathbf{B}}$ or $\hat{\mathbf{C}}$. For example, a new reduced input matrix $\hat{\mathbf{B}}$ can be determined by minimizing

$$\begin{aligned} &\min_{\hat{\mathbf{B}}} \quad \sum_{k=1}^{K} \| \tilde{y}(k) - \hat{y}(k) \|_2 \\ &\text{subject to} \quad \Lambda \text{ given by (27) and } \hat{\mathbf{C}} \text{ given by (29).} \end{aligned} \tag{30}$$

Such a minimization problem can be solved by the following procedure. Note that the reduced input matrix $\hat{\mathbf{B}}$ is of the form

$$\hat{\mathbf{B}} = \begin{bmatrix} \hat{b}_1 \\ \hat{b}_2 \\ \vdots \\ \hat{b}_{n_1'-1} \\ \hat{b}_{n_1'} \\ \hat{b}_{n_1'+1} \\ \vdots \\ \hat{b}_{n'} \end{bmatrix} = \begin{bmatrix} \hat{b}_1^R + \mathrm{j}\hat{b}_1^I \\ \hat{b}_2^R - \mathrm{j}\hat{b}_1^I \\ \vdots \\ \hat{b}_{n_1'-1}^R + \mathrm{j}\hat{b}_{n_1'-1}^I \\ \hat{b}_{n_1'-1}^R - \mathrm{j}\hat{b}_{n_1'-1}^I \\ \hat{b}_{n_1'+1} \\ \vdots \\ \hat{b}_{n'} \end{bmatrix}, \tag{31}$$

where $\hat{b}_i^R$ and $\hat{b}_i^I$ are the real part and the imaginary parts of $\hat{b}_i$ for $i = 1, 3, \ldots, n_1' - 1$, respectively, and $\mathrm{j} = \sqrt{-1}$. The response corresponding to a unit of $\hat{b}_i^R$ is computed by

$$\begin{aligned} \eta_i^R(k+1) &= \Lambda\eta_i^R(k) + I_i^R u(k), \\ y_{\hat{b}_i^R}(k) &= \hat{\mathbf{C}}\eta_i^R(k), \quad i = 1, 3, \ldots, n_1' - 1, \end{aligned} \tag{32}$$

where $I_i^R \in R^{n' \times 1}$ and its $(2i-1)$th and $2i$th elements are unity and the rest of the elements are zero. The response corresponding to a unit of $\hat{b}_i^I$ is computed by

$$\begin{aligned} \eta_i^I(k+1) &= \Lambda\eta_i^I(k) + I_i^I u(k)\,, \\ y_{\hat{b}_i^I}(k) &= \hat{\mathbf{C}}\eta_i^I(k), \quad i = 1, 3, \ldots, n_1' - 1, \end{aligned} \tag{33}$$

where $I_i^I \in R^{n' \times 1}$ and its $(2i-1)$th element is j and $2i$th element is $-\mathrm{j}$ and the rest of the elements are zero. The response corresponding to a unit of $\hat{b}_i$ for $i \geqslant n_1' + 1$ is computed by

$$\eta_i(k+1) = \Lambda\eta_i(k) + I_i u(k), \quad y_{\hat{b}_i}(k) = \hat{\mathbf{C}}\eta_i(k), \tag{34}$$

where $I_i \in R^{n' \times 1}$ and its ith element is unity and the rest of the elements are zero. Now, the linear relationship between $y(k)$ and the elements of $\hat{\mathbf{B}}$ is given as

$$\begin{aligned} \tilde{y}(k) &= \sum_{i=1,3}^{n_i'-1} [y_{\hat{b}_i^R}(k)\hat{b}_i^R + y_{\hat{b}_i^I}(k)\hat{b}_i^I] + \sum_{i=n_1'+1}^{n'} y_{\hat{b}_i}(k)\hat{b}_i \\ &= \Phi(k)\Theta, \end{aligned} \tag{35}$$

where $\Phi(k) \in R^{m \times n'}$ and $\Theta \in R^{n' \times 1}$ are defined as

$$\begin{aligned} \Theta(k) &= [y_{\hat{b}_1^R}(k)\ \ y_{\hat{b}_1^I}(k) \cdots y_{\hat{b}_{n_1'-1}^R}(k)\ \ y_{\hat{b}_{n_1'-1}^I}(k)\ \ y_{\hat{b}_{n_1'+1}}(k) \cdots y_{\hat{b}_{n'}}(k)], \\ \Theta &= [\hat{b}_1^R\ \ \hat{b}_1^I \cdots \hat{b}_{n_1'-1}^R\ \ \hat{b}_{n_1'-1}^I\ \ \hat{b}_{n_1'+1} \cdots \hat{b}_{n'}] \end{aligned} \tag{36}$$

respectively. The LS solution for the elements of the matrix $\hat{\mathbf{B}}$ is

$$\Theta = \Phi^+ \tilde{y}, \tag{37}$$

where $\Phi \in R^{(K \times m) \times n'}$ and $\tilde{y} \in R^{(K \times m) \times 1}$ are of the forms

$$\Phi = \begin{bmatrix} \Phi(1) \\ \Phi(2) \\ \vdots \\ \Phi(K) \end{bmatrix} \quad \text{and} \quad \tilde{y} = \begin{bmatrix} \tilde{y}(1) \\ \tilde{y}(2) \\ \vdots \\ \tilde{y}(K) \end{bmatrix} \tag{38}$$

respectively. In a similar manner, a new output matrix $\hat{\mathbf{C}}$ can be computed by solving the following minimization problem:

$$\begin{aligned} &\min_{\hat{\mathbf{C}}} \quad \sum_{k=1}^{K} \| \tilde{y}(k) - \hat{y}(k) \|_2 \\ &\text{subject to} \quad \Lambda \text{ given by (27) and } \hat{\mathbf{B}} \text{ given by (28).} \end{aligned} \tag{39}$$

6. IDENTIFICATION EXPERIMENTS

This section presents the experiment design, data preprocessing, identification results, and observations based on the results. Design of experiments involves selection of sampling frequency, excitation methods, and exciting signals.

In a previous study [20], it was found that the excitation generated by the motor can induce up to the third vibratory mode of the arm. If the arm is modelled as a cantilever beam, its first three natural frequencies are 8·90, 24·58 and 48·20 Hz respectively. Therefore, the sampling frequency was chosen to be 300 Hz in order to capture the significant modal information. Although the computer system is capable of achieving a higher sampling frequency, a further increase of the sampling frequency will result in a drastic increase of the data and computational time. When the sampling frequency is chosen to be too high, it may cause the eigenvalue of a lightly damped mode to move too close to the unit circle.

Two different experiments were conducted, namely, open-loop and closed-loop experiment. In the open-loop experiment, an exciting command is generated in the computer and sent to the power amplifier through the D/A channel. Exciting signals must be properly chosen to provide sufficiently rich excitation over the frequency band of the system dynamics. Four types of signals were tested: square waveform, varying square waveform, periodic random, and random signal. In theory, random signal is an ideal choice because it is persistently exciting. However, for the system under study, it was found that the responses to a random input were quite noisy and contained many spikes. When such data were used in identification, the models obtained have larger prediction errors than those obtained using the data from a square or varying square waveform. It is believed that the random excitation magnifies the system non-linearities such as gear backlash and Coulomb friction due to frequent sudden changes in input magnitude and direction. After many trails, it was found that the varying square waveform was a best choice for the present system. The varying square waveform consists of a series of positive and negative pulses. The magnitude of the pulse was prescribed and its period randomly varied between 0·25 and 1·5 s. Figure 2 shows a typical varying square waveform. In what follows, only the results with the excitation of the varying square waveforms are reported.

In the closed-loop experiment, the angular position is fed back and compared with a reference position. The exciting signal is proportional to the error between the reference position and actual position. The reference position was specified in the following way: In the beginning, a reference of 3 v (35° of hub rotation) was used until the actual angular

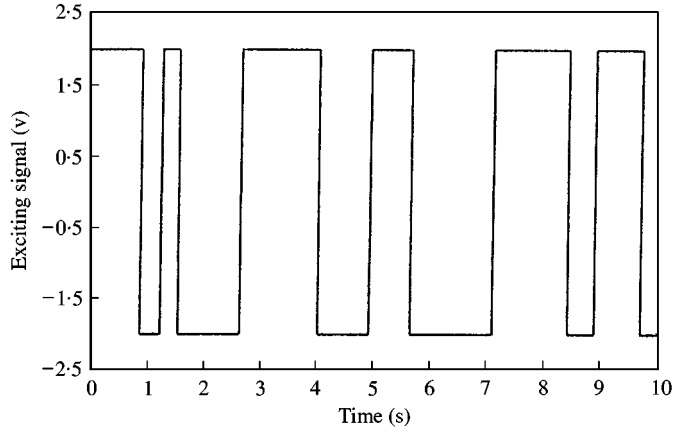

Figure 2. Varying square waveform used as the exciting command in the open-loop experiment.

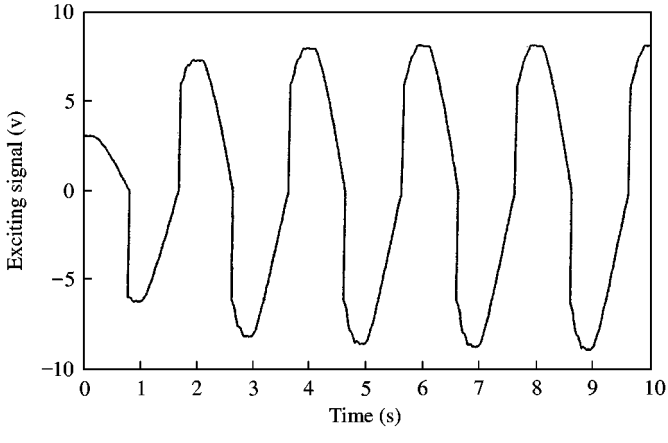

Figure 3. Resultant exciting command used in the closed-loop experiment.

position exceeded 3 v. As soon as the actual angular position exceeded 3 v, the reference was changed into -3 v (-35° of hub rotation) and remained so until the actual angular position became less than -3 v. As soon as the measured angular position became less than -3 v, the reference was reverted to 3 v. The process continued until it was terminated. Such an exciting strategy was devised in order to have a sufficient excitation while the range of hub rotation is limited. Figure 3 shows a typical resultant exciting command from the closed-loop experiment.

The measured outputs were preprocessed in the following ways. The sampled outputs were passed through a second order Butterworth filter with a cut-off frequency of 50 Hz. The bias in each of the measured outputs was removed. The strain gauge signals were forced to be zero mean. The initial outputs were forced to be zero, i.e., $\tilde{y}(1) = 0$. All the four outputs were scaled to ensure that their maximum magnitudes are equal to the maximum magnitude of the input. The scaling is needed in order to avoid the discrimination according to the data magnitudes in the computation [6]. The final identified output matrix $\hat{\mathbf{C}}$ or $\bar{\mathbf{C}}$ were obtained through an unscaling operation using the scaling factors.

The identification results were evaluated in several ways. The ratio of the root-mean-squared (RMS) prediction errors is defined as

$$\delta_i = \frac{\mathrm{RMS}(\tilde{y}_i - \hat{y}_i)}{\mathrm{RMS}(\tilde{y}_i)} \quad i = 1, \ldots, 4 \quad \text{and} \quad \bar{\delta} = \sum_{i=1}^{4} \delta_i / 4, \tag{40}$$

where the subscripts 1, 2, 3, and 4 denote the angular position, angular speed, base gauge signal, and middle gauge signal respectively. The natural frequencies and damping ratios are computed from the eigenvalues of the identified transition matrix $\bar{\mathbf{A}}$. The ith natural frequency f_i and damping ratio ζ_i are related to the ith complex eigenvalue by

$$\lambda_i = \mathrm{e}^{(-\zeta_i + j\sqrt{1-\zeta_i^2})2\pi f_i \Delta t} \quad \text{for } i = 1, 3, \ldots, n_1 - 1.$$

In addition, the identified models were validated in two ways. In a data projection validation, the duration of the simulated response was twice as long as that of the data used in the model identification. The data projection validation checks the model's ability to generate the responses that were not used in the model identification. In a data matching validation, the magnitude of the input applied to a model was different from that of the input used in the model identification. The data matching validation tests the linearity of the system and the adaptability of the identified model.

Knowledge of the mathematical model is helpful to determine a minimum model order. The system dynamics includes the effects of the flexible arm and motor plus the transmission train. For the first three vibratory modes of the arm, six modes are needed. The motor and transmission system may be represented by two or three modes depending on the extent of modelling. Therefore, the minimum order of the model is 8 or 9. However, the non-linearities of the system introduce additional computational modes. If the model order is not sufficiently large, some significant structural modes may not be captured. On the other hand, the singular values of the matrix $\mathbf{Y}\mathbf{U}^{\perp}\mathbf{Y}^{\mathrm{T}}$ present some information about the dynamics [22]. Shown in Figure 4 are the first 50 singular values of the matrix $\mathbf{Y}\mathbf{U}^{\perp}\mathbf{Y}^{\mathrm{T}}$ formed by data set 1 in Table 1. It is seen that there are several visible plateaus up to the 25th singular value. In identification, $n = 25$ was considered as an upper bound for the model order.

The identification computation was conducted using MATLAB. The data length K was chosen to be $K = 1500$ or the duration of the data was 5 s. As a general guideline, the block

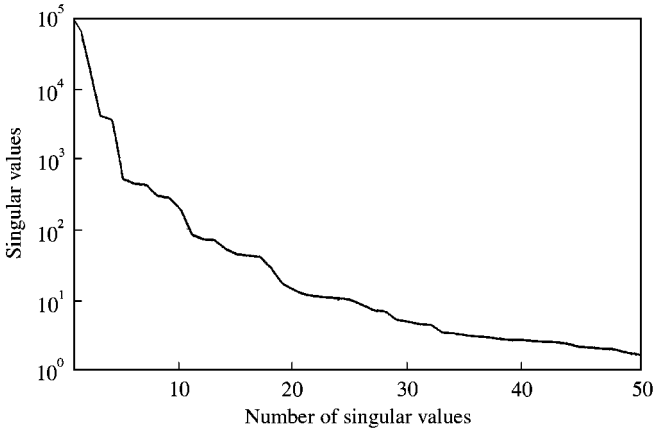

Figure 4. The first 50 singular values of matrix $\mathbf{Y}\mathbf{Y}^{\mathrm{T}} - \mathbf{Y}\mathbf{U}^{\mathrm{T}}(\mathbf{U}\mathbf{U}^{\mathrm{T}})^{+}(\mathbf{Y}\mathbf{U}^{\mathrm{T}})^{\mathrm{T}}$ using data set 1.

TABLE 1

Data sets used in identification

Set no.	Testing conditions
1	Open loop, input level = 1·5 v
2	Open loop, input level = 2 v
3	Closed loop, proportional gain = 0·7
4	Closed loop, proportional gain = 1

TABLE 2

Prediction errors of the identified models using data set 1

n	δ_1	δ_2	δ_3	δ_4	$\bar{\delta}$	No. of real λ_i/stable
13	0·1238	0·2608	0·3315	0·6212	0·3343	$1/N^{\dagger}$, $\lambda_{13} = 1{\cdot}0008$
14	0·1330	0·2412	0·2754	0·5192	0·2922	$2/Y$
15	0·1118	0·2524	0·3435	0·6367	0·3361	$1/N$, $\lambda_{13} = 1{\cdot}0006$
16	0·1013	0·2316	0·3108	0·5658	0·3024	$2/Y$
17	0·0768	0·2454	0·3193	0·5579	0·2999	$3/N$, $\lambda_{17} = 1{\cdot}0013$
18	0·0655	0·2351	0·2775	0·5288	0·2767	$2/Y$
19	0·1456	0·2506	0·3030	0·5577	0·3142	$1/N$, $\lambda_{19} = 1{\cdot}0010$
20	0·0456	0·1901	0·2966	0·5492	0·2704	$2/N$, $\lambda_{20} = 1{\cdot}0011$

[†]There is one real eigenvalue and the model is not stable.

row dimension q of the Hankel matrices must be greater than the model order, i.e., $q > n$. In the results reported below, $q = 5n$ was used and then $d = K - q + 1$.

Numerous experiments were carried out [23]. Limited by the space available, only selected results from four sets of the data are presented below. The information of the data sets is given in Table 1. Table 2 lists some results using data set 1. Among the four outputs, the identified models give the best fit for the angular position and the worst fit for the middle gauge signal. The identified models tend to be unstable and the unstable models contain one real eigenvalue that is greater than unity. Figure 5 shows the data projection validation using the 13th order model. In all the figures used, solid lines represent the measured outputs and dotted lines represent the simulated ones. The display duration is divided into two periods and the data of the first 5 s period were used in identification. It is noted that the simulated angular position deviates from the measured one after 5 s. For the strain gauge signals, the simulated outputs agree well with the measured ones during the first 5 s and show a visible departure from the measured ones after 5 s. The main reason for mismatching in the second period is that one of the identified rigid modes is unstable.

Table 3 lists some results using data set 2. Compared with the results using data set 1, the models seem to have poorer fits for the angular position and velocity and better fits for the strain gauge signals. Figure 6 shows the data projection validation using the 14th order model (to save space, only two outputs are shown). This model is stable. It is seen that the simulated outputs still follows the measured ones in the second period.

Figure 7 shows a data matching validation where the input of data set 1 was applied to the 14th order model identified using data set 2. The model is capable of generating the strain gauge signals that agree with the measured ones. For the angular position, there is a visible disagreement between the simulated one and measured one. More experiments

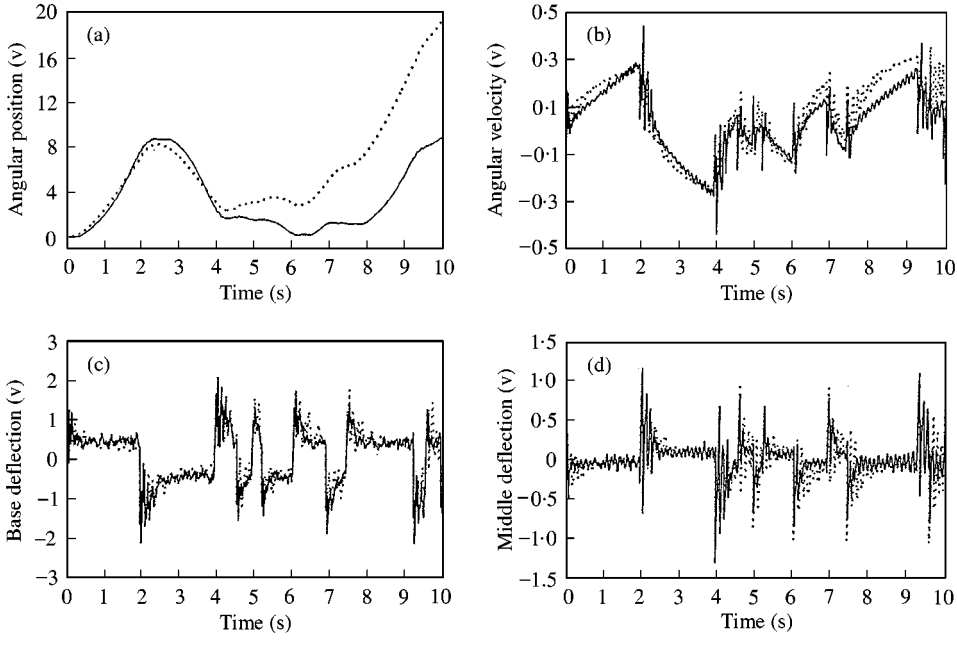

Figure 5. Comparison of the measured outputs and simulated ones by the 13th order model using data set 1: (——), measured; (·····), simulated. (a) Angular position; (b) angular velocity; (c) base deflection; (d) middle deflection.

TABLE 3

Prediction errors of the identified models using data set 2

n	δ_1	δ_2	δ_3	δ_4	$\bar{\delta}$	No. of real λ_i/stable
13	0·3041	0·2888	0·2652	0·4780	0·3340	$1/N$, $\lambda_{13} = 1{\cdot}0012$
14	0·1755	0·2476	0·2424	0·4571	0·2806	$2/Y$
15	0·2817	0·2528	0·2356	0·4842	0·3136	$1/N$, $\lambda_{15} = 1{\cdot}0010$
16	0·1589	0·2343	0·2185	0·4129	0·2561	$2/Y$
17	0·2396	0·2474	0·2434	0·4477	0·2945	$1/N$, $\lambda_{17} = 1{\cdot}0011$
18	0·1766	0·2402	0·2352	0·4412	0·2733	$2/Y$
19	0·2846	0·2489	0·2424	0·4853	0·3153	$1/N$, $\lambda_{19} = 1{\cdot}0011$
20	0·1733	0·2248	0·2089	0·3914	0·2496	$2/N$, $\lambda_{20} = 1{\cdot}0001$

have shown that when the input with a magnitude of 1 v was applied to this model, the simulated angular position disagrees with the measured one more visibly. This indicates that in the open-loop experiment, the system exhibits some degree of nonlinearity.

The results from data set 4 are given in Table 4. In general, the models identified in the closed-loop experiments have smaller prediction errors than those from the open-loop experiments, especially for the angular position and velocity. The models tend to be stable. For an unstable model, there is a pair of complex eigenvalues that are outside the unit circle. Figure 8 shows a data projection validation using the 13th order model. The model is capable of predicting the outputs beyond the length used for the model identification. Figure 9 gives a comparison for the 20th order model. It is noted that, even if the identified model is slightly unstable, the simulated outputs still follow well the measured ones.

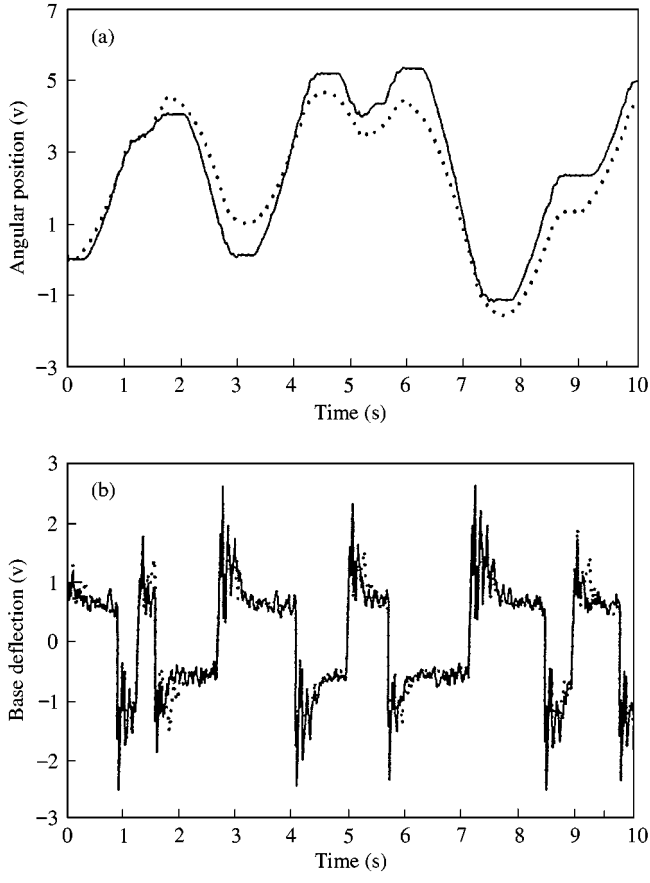

Figure 6. Comparison of the measured outputs and simulated ones by the 14th order model using data set 2: (——), measured; (·····), simulated. (a) Angular position; (b) base deflection.

Figure 10 presents a data matching validation. In this case, the input from data set 3 was applied to the 13th order model identified using data set 4. It is seen that, although there is magnitude mismatch, the simulated outputs follow the variations of the measured ones well.

As the first example of the model reduction, consider the 13th order model using data set 2. This is an unstable model. To force it to become stable, the unstable real eigenvalue λ_{13} was modified to be $\lambda_{13} = 1$. Then the MRMs for all the modal responses were evaluated. The MRMs and their ranking are given in Table 5. The corresponding MRVs and their ranking are also given for comparison. In addition, the table lists the corresponding natural frequencies and damping ratios for the complex modes. According to the MRMs, a reduced model of order 7 should retain modes: 1/2, 7/8, 9/10, 13. The prediction errors of this truncated model are given in Table 6. Using the proposed updating algorithm to recalculate the input matrix results in an updated reduced order model. As indicated in Table 6, the updated model is able to achieve a better model accuracy than the original one in terms of the average prediction error $\bar{\delta}$. A comparison of the outputs for the three different models is given in Figure 11. If the model was reduced by the MSV ranking, a model of order 7 should contain modes: 1/2, 5/6, 7/8, 13. It is noted that a pair of complex modes 9/10 was considered as less important by the MSVs. This pair of complex modes is associated with the motor dynamics. Its pulse response dies quickly because the modes are heavily damped.

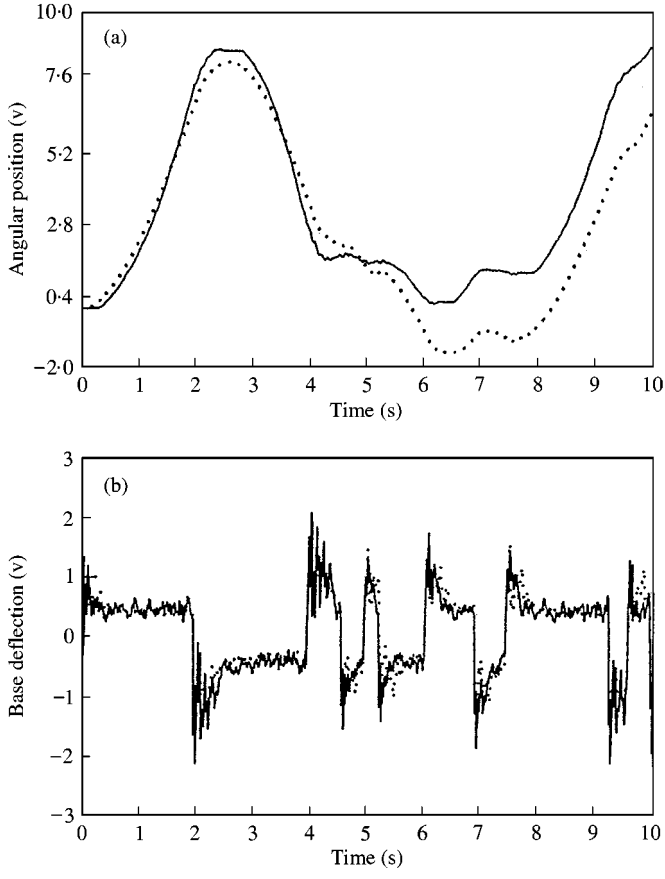

Figure 7. Comparison of the measured outputs and simulated ones in the data matching validation. The input of data set 1 was applied to the 14th order model using data set 2: (——), measured; (·····), simulated. (a) Angular position; (b) base deflection.

TABLE 4

Prediction errors of the identified models using data set 4

n	δ_1	δ_2	δ_3	δ_4	$\bar{\delta}$	No. of real λ_i/stable
13	0·0737	0·1759	0·2346	0·4460	0·2325	$1/Y$
14	0·0697	0·1783	0·2554	0·5050	0·2521	$0/Y$
15	0·0825	0·1876	0·2588	0·5208	0·2624	$1/N$, $\lambda_{13,14} = 1{\cdot}0001 \pm$j0·01541
16	0·1319	0·1776	0·3328	0·6112	0·3134	$0/N$, $\lambda_{15,16} = 1{\cdot}0004 \pm$j0·01546
17	0·0844	0·1811	0·2739	0·4897	0·2573	$1/Y$
18	0·0631	0·1777	0·2287	0·4629	0·2331	$0/N$, $\lambda_{17,18} = 1{\cdot}0001 \pm$j0·01893
19	0·0657	0·1699	0·2540	0·4780	0·2419	$1/Y$
20	0·0682	0·1717	0·2240	0·4589:	0·2307	$0/Y$, $\lambda_{19,20} = 1{\cdot}0004 \pm$j0·01959

The prediction errors for the reduced model and updated model based on the MSVs are also listed in Table 6. The errors in the reduced model are large and the updating scheme fails to improve the model.

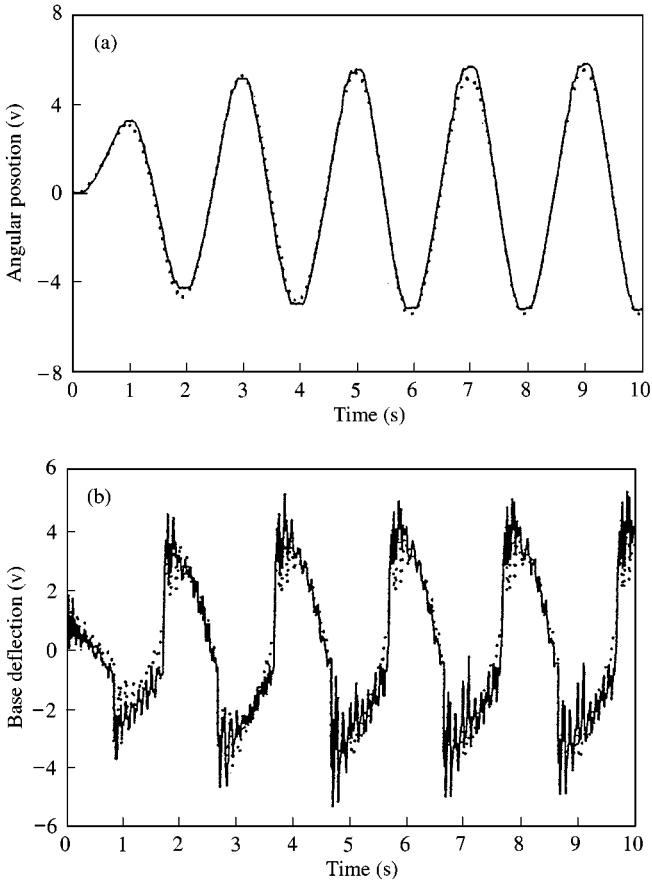

Figure 8. Comparison of the measured outputs and simulated ones by the 13th order model using data set 4: (——), measured; (·····), simulated. (a) Angular position; (b) base deflection.

In the second example, the 19th order model using data set 2 was tested. Table 7 lists the MRMs and MSVs for all the modes. According to the MRMs, a model of order 11 should retain modes: 5/6, 11/12, 13/14, 15/16, 17/18, 19. Table 8 lists the prediction errors of the reduced model and the model with a recalculated input matrix respectively. It is seen that the updated model is better than the original model. If the MSVs are used to select the dominant modes, the modes that should be kept are 1/2, 5/6, 9/10, 11/12, 13/14, 19. It is noted that the pair of complex modes 1/2 is considered to be important. By examining the natural frequencies, this is known that this pair of complex modes is associated with the third vibratory mode of the arm. An extensive experiment has indicated that the third vibratory mode has an insignificant contribution to the total response. However, this set of modes has a dominant presence in a pulse response because of a low damping and high-frequency nature. As indicated in Table 8, the updated model reduced by the MSV ranking is unacceptable. The prediction errors for the angular position and velocity cannot be improved effectively because the pair of complex modes 15/16 has been excluded.

If the model order is further reduced to 7 according to the MRMs, the reduced model will not contain the dynamics of the second vibratory mode represented by the pair 5/6. Although this seventh order model still represents the basic system dynamics, it may not be acceptable for controller design. This indicates a limitation of the MRM index. In such

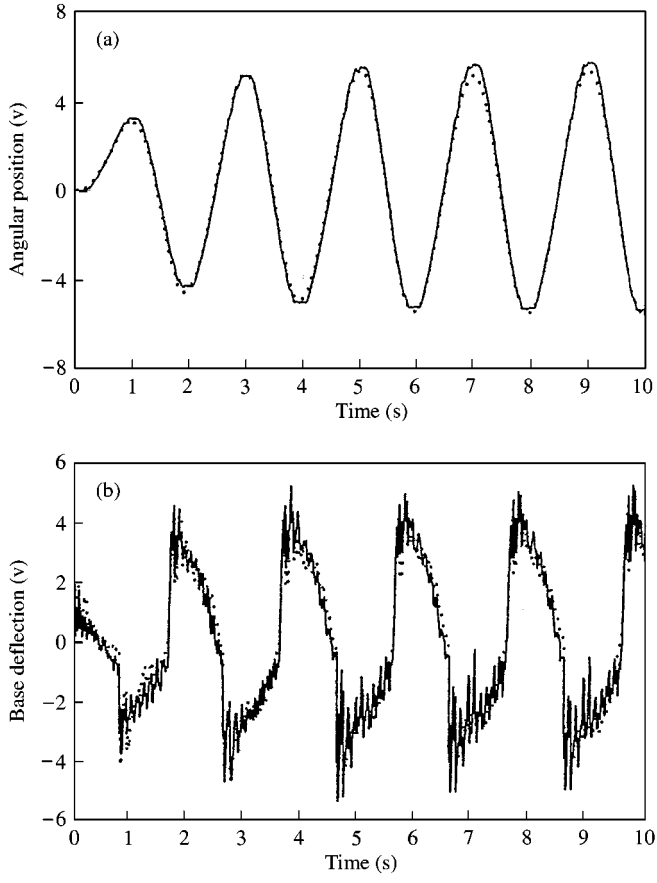

Figure 9. Comparison of the measured outputs and simulated ones by the 20th order model using data set 4: (——), measured; (·····), simulated. (a) Angular position; (b) base deflection.

a case, a prior knowledge about the system dynamics is useful to make a decision. Table 8 lists the prediction errors for model II which consists of modes: 5/6, 11/12, 15/16, 19. These modes were selected based on both their MRM values and modal information. As indicated in Table 8, the updated model achieves a model accuracy that is close to that of the original model. For the angular position, the model fits the measured value even better than the original model. A comparison of the frequency responses for the original model, updated model I, and updated model II is given in Figure 12. The original model has to use more modes to represent the dynamics around the first two natural frequencies of the arm. The frequency response of updated model I shows a sharp peak at the second natural frequency and two peaks around the first natural frequency. Although the frequency response of updated model II appears simpler, it still captures the main characteristics of the dynamics in the lower frequency region.

The models from the closed-loop experiments were also used to study the model reduction. As an example, Table 9 gives the MRMs and MSVs for the 15th order model using data set 4. According to the MRMs, a reduced model of order 7 should retain modes: 3/4, 7/8, 13/14, 15. The mean prediction error for the updated model is slightly greater than that for the original model (Table 10). In general, in the closed-loop experiments, although recalculation of the input matrix for a properly reduced model makes the prediction errors

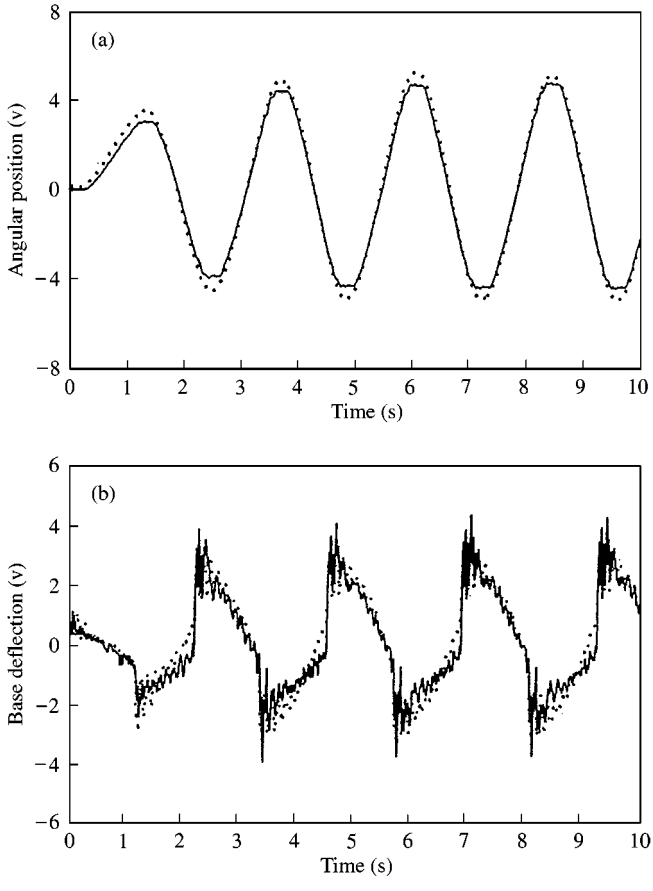

Figure 10. Comparison of the measured outputs and simulated ones in the data matching validation. The input of data set 3 was applied to the 13th order model identified using data set 4: (——), measured; (·····), simulated. (a) Angular position; (b) base deflection.

TABLE 5

Comparison of the MRMs and MSVs for the 13*th order model given in Table* 2

Modes	MRMs/rank	MSVs/rank	f_i	ζ_i
1/2	0·2085/4	1·1269/4	22·39	0·0477
3/4	0·0848/6	0·9515/5	18·30	0·0244
5/6	0·0760/7	1·2110/2	9·623	0·0174
7/8	0·4110/2	1·1515/3	8·120	0·0784
9/10	0·4822/1	0·5293/7	0·3578	0·7881
11/12	0·1789/5	0·5597/6	3·121	0·1390
13	0·3593/3	1·3696/1	—	—

smaller, the updated model accuracy is not as good as its original one. If the MSVs are used, a model of order 8 contains modes: 3/4, 5/6, 7/8, 13/14. In this case, mode 15 is excluded. This mode is associated with the rigid-body motion. As expected, the prediction errors from the updated model (model II in Table 10) are unacceptable.

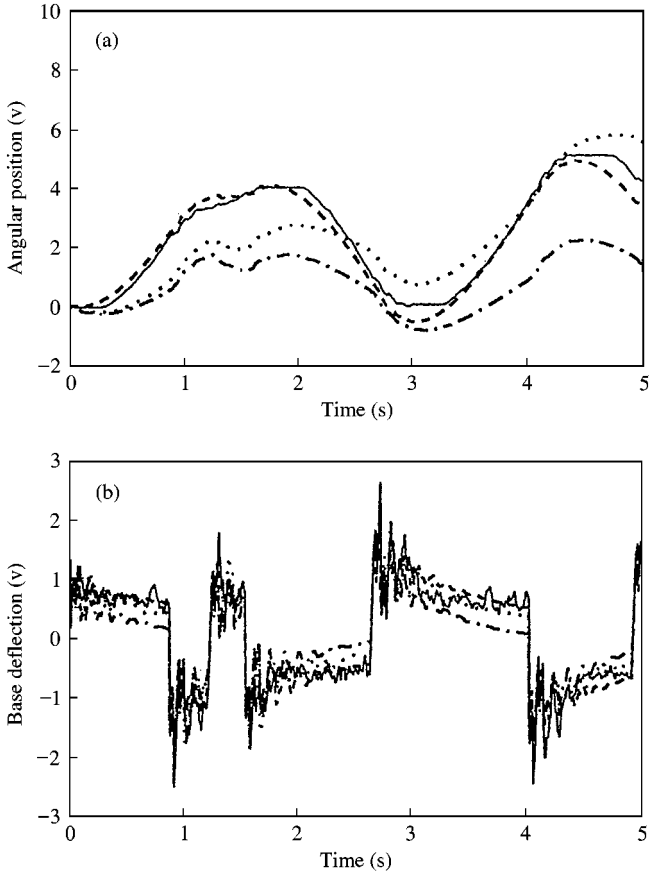

Figure 11. Comparison of the measured outputs and outputs generated by the different models: (——), measured; (·····), original model; (—·—·—), reduced model; (– – – –), updated model. (a) Angular position; (b) base deflection.

TABLE 6

Prediction errors of the original, reduced, and updated models for the model given in Table 5. Model I consists of modes: 1/2, 7/8, 9/10, 13. Model II consists of modes: 1/2, 5/6, 7/8, 13

Model	n	δ_1	δ_2	δ_3	δ_4	$\bar{\delta}$
Original	13	0·3041	0·2888	0·2652	0·4780	0·3340
I, reduced	7	0·6223	0·2990	0·4195	0·5587	0·4749
I, updated	7	0·1048	0·2745	0·2778	0·5448	0·3005
II, reduced	7	0·7559	0·8535	0·4307	0·5294	0·6424
II, updated	7	0·6122	0·7766	0·3897	0·5164	0·5737

7. CONCLUSION

The ORSE algorithm has been applied to control-model identification for the system that involves both rigid-body motion and structural vibration. The study has successfully addressed several important issues in the experiment.

TABLE 7

Comparison of the MRMs and MSVs for the 19*th order model given in Table* 3

Modes	MRMs/rank	MSVs/rank	f_i	ζ_i
1/2	0·0880/8	1·1328/3	46·66	0·0232
3/4	0·0316/9	0·7920/7	22·97	0·0156
5/6	0·1468/6	0·9688/5	21·38	0·0483
7/8	0·0076/10	0·4042/10	17·44	0·0130
9/10	0·1134/7	1·0399/4	10·62	0·0287
11/12	0·1725/4	1·1668/2	8·917	0·0289
13/14	0·3041/3	0·8602/6	6·974	0·1201
15/16	0·5053/1	0·5420/8	0·424	0·8407
17/18	0·1648/5	0·4594/9	2·5480	0·1978
19	0·4321/2	1·5018/1	—	—

TABLE 8

Prediction errors of the original, reduced, and updated models for the model given in Table 7. Model I consists of modes: 5/6, 11/12, 13/14, 15/16, 17/18, 19. Model II consists of modes: 5/6, 11/12, 15/16, 19. Model III consists of modes: 1/2, 5/6, 9/10, 11/12, 13/14, 19

Model	n	δ_1	δ_2	δ_3	δ_4	$\bar{\delta}$
Identified	19	0·2846	0·2489	0·2424	0·4853	0·3153
I, reduced	11	0·5818	0·2680	0·2562	0·5941	0·4250
I, updated	11	0·1096	0·2627	0·2515	0·5161	0·2850
II, reduced	7	0·5799	0·4065	0·7688	0·8387	0·6485
II, updated	7	0·0900	0·3115	0·3717	0·6369	0·3525
III, reduced	11	0·7191	0·9470	0·3810	0·5504	0·6494
III, updated	11	0·6124	0·7921	0·3844	0·5405	0·5823

1. With regard to the methods to excite the system, it has been found that in the open-loop experiment, the range of hub motion is difficult to be regulated and the responses are affected by the system non-linearities. On the other hand, the closed-loop experiment tends to minimize non-linear influence and allows to use large input level. In general, the data from the closed-loop experiments result in more accurate models than those from the open-loop experiment.

2. For the system under study, a proper selection of exciting signal is important. The study has shown that the varying square waveform is the best choice among the four different exciting signals. Such an excitation can fully excite both the rigid-body motion and structural vibration while keeping the non-linear effects minimum.

3. Two model validation methods have been used. The data projection validation checks a model's ability to generate the responses that were not used in the model identification. The data matching validation tests the linearity of the system and the adaptability of the identified model.

4. Several data preprocessing operations have been used. The study has shown that these operations are critical to ensure a successful application of the ORSE algorithm.

A model reduction technique had been proposed and successfully applied. An index named as MRM index has been proposed to quantify the contribution of individual modes.

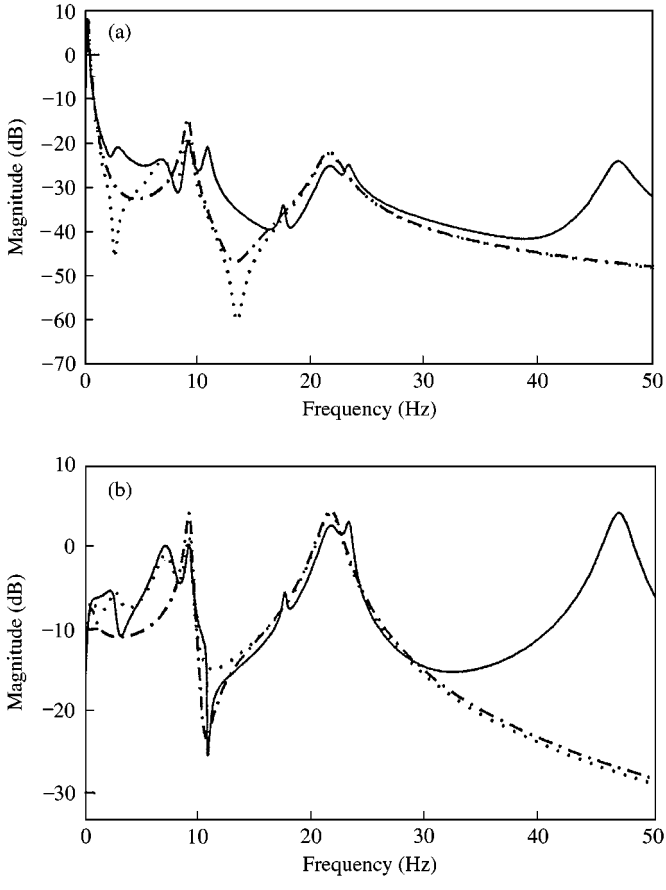

Figure 12. Comparison of the frequency responses for the different models: (——), original model; (·····), updated reduced model I; (—·—·—), updated reduced model II. (a) Angular position; (b) base deflection.

TABLE 9

Comparison of the MRMs and MSVs for the 15*th order model given in Table* 4

Modes	MRMs/rank	MSVs/rank	f_i	ζ_i
1/2	0·0788/8	0·8999/7	23·02	0·0116
3/4	1·6633/4	2·3363/4	21·55	0·0314
5/6	0·9271/5	2·6721/3	9·444	0·0124
7/8	2·1342/3	2·8573/1	8·330	0·0275
9/10	0·4636/6	0·9102/6	1·871	0·0507
11/12	0·1542/7	0·3257/8	0·737	0·0571
13/14	4·7104/1	2·7572/2	0·1926	0·4582
15	3·9447/2	1·1483/5	—	—

The study has shown that the new measure is reliable when the order of an original model is low or moderate. When the model order is high, determination of the mode dominance should be based on both the MRM values and modal information available. Ranking the mode dominance according to the modal responses provides a more meaningful insight to

TABLE 10

Prediction errors of the original, reduced, and updated models for the model given in Table 9. Model I consisted of modes: 3/4, 7/8, 13/14, 15. Model II consisted of modes: 3/4, 5/6, 7/8, 13/14

Model	n	δ_1	δ_2	δ_3	δ_4	$\bar{\delta}$
Original	15	0·0825	0·1876	0·2588	0·5208	0·2624
I, reduced	7	0·0685	0·1898	0·4037	0·6509	0·3282
I, updated	7	0·0806	0·2121	0·2799	0·6013	0·2935
II, reduced	8	0·2481	0·2965	1·1257	1·4886	0·7897
II, updated	8	0·3106	0·3021	0·5959	0·7664	0·4938

the model than the balanced realization technique. In modal co-ordinates, it is easy to modify a model to ensure model stability.

A model-updating scheme has been proposed. The experimental study has indicated that if the truncated model preserves the main modal information, the proposed updating scheme can effectively improve the accuracy of a reduced order model. If a model is not properly reduced or some of the significant system modes are missing, the method cannot produce a satisfactory result.

ACKNOWLEDGMENTS

The authors wish to acknowledge the support of the National Science and Engineering Research Council of Canada under grant No. OGP-0184068. Technical assistance from Dr K. Natarajan is greatly appreciated.

REFERENCES

1. J.-N. JUANG 1994 *Applied System Identification* Englewood Cliffs, NJ: Prentice-Hall.
2. J.-N. JUANG and R. S. PAPPA 1985 *Journal of Guidance* **8**, 620–627. An eigensystem realization algorithm for modal parameter identification and model reduction.
3. R. S. PAPPA and J.-N. JUANG 1988 *Sound and Vibration* **22**, 30–34. Some experience with the eigensystem realization algorithm.
4. R. W. LONGMAN and J. JUANG 1988 *Journal of Guidance, Control and Dynamics* **12**, 647–652. A recursive form of the eigensystem realization algorithm.
5. J.-N. JUANG, M. PHAN, L. G. HORTA and R. W. LONGMAN 1993 *Journal of Guidance, Control, and Dynamics* **16**, 320–329. Identification of observer/kalman filter markov parameters: theory and experiments.
6. K. LIU and D. W. MILLER 1995 *American Society of Mechanical Engineers Journal of Dynamic Systems, Measurement, and Control* **117**, 608–618. Time domain state space identification of structural systems.
7. A. M. KING, U. B. DESAI and R. E. SKELETON 1988 *Automatica* **24**, 507–515. A generalized approach to q-markov covariance equivalent realizations for discrete systems.
8. J.-N. JUANG 1997 *Journal of Guidance, Control, and Dynamics* **20**, 67–73. Unification of several system realization algorithms.
9. M. VERHAEGEN and P. DEWILDE 1992 *International Journal of Control* **56**, 1187–1210. Subspace model identification: Part 1. The output-error state-space model identification class of algorithms.
10. H. M. KIM and H. H. DOIRON 1992 *Sound and Vibration* **26**, 24–30. On-orbit model identification of large space structures.
11. J.-S. LEW, J.-N. JUANG and R. W. LONGMAN 1993 *Journal of Sound and Vibration* **167**, 461–480. Comparison of several system identification methods for flexible structures.

12. B. MOORE 1981 *IEEE Transactions on Automatic Control* **26**, 17–31. Principal component analysis in linear systems: controllability, observability, and model reduction.
13. J.-N. JUANG and R. W. LONGMAN 1999 *NASA Technical Memorandum*, *NASA*-99-*TM* 209711. Optimized system identification.
14. D. M. ROVNER and R. H. CANNON, JR. 1987 *The International Journal of Robotics Research* **6**, 3–19. Experiments toward on-line identification and control of a very flexible one-link manipulator.
15. S. YURKOVICH, F. E. PACHECO and A. P. TZES 1989 *IEEE Transactions on Automatic Control* **34**, 1300–1304. On-line frequency domain information for control of a flexible-link robot with varying payload.
16. S. YURKOVICH, A. P. TZES, I. LEE, and K. L. JILLSLEY 1990 *Proceedings of the IEEE International Conference Robotics and Automation, Cincinnati*, *OH*, 1626–1631. Control and system identification of a two-link flexible manipulator.
17. A. P. TZES and S. YURKOVICH 1991 *The International Journal of Robotics Research* **10**, 515–527. Application and comparison of on-line identification methods for flexible manipulator control.
18. K. L. HILLSLEY and S. YURKOVICH 1993 *Dynamics and Control* **3**, 261–280. Vibration control of a two-link flexible robot arm.
19. A. FUJIMORI, P. N. NIKIFORUK and E. KODA 1995 *Journal of Systems and Control Engineering* **209**, 13–20. Modeling of a flexible arm using system identification and model reduction.
20. S. YU 1997 *Master's Thesis*, *Lakehead University*, *Thunder Bay*, *Canada*. Control of flexible-link manipulator.
21. J.-N. JUANG 1997 *Journal of Guidance*, *Control*, *and Dynamics* **20**, 492–500. System realization using information matrix.
22. K. LIU 1996 *Journal of Sound and Vibration* **197**, 387–402. Modal parameter estimation using the state space method.
23. X. SUN 2000 *Master's Thesis*, *Lakehead University*, *Thunder Bay*, *Canada*. System identification and control of a flexible-link manipulator.